Lattice and continuum theories of Huang scattering

1999 J. Phys.: Condens. Matter 11 3075

(http://iopscience.iop.org/0953-8984/11/15/013)

J. Phys.: Condens. Matter **11** (1999) 3075–3090. Printed in the UK PII: S0953-8984(99)97589-6

Lattice and continuum theories of Huang scattering

R I Barabash†, J S Chung‡ and M F Thorpe§

Physics and Astronomy Department and Center for Fundamental Materials Research, Michigan State University, East Lansing, MI 48824-1116, USA

Received 15 September 1998

Abstract. The predicted x-ray and neutron scattering by random semiconductor alloys $A_{1-x}B_xC$ with the zinc-blende structure has been analysed using direct simulation of the scattering from the atoms in the lattice, and also using a continuum theory. This initial work focuses on the *special* case of the single-impurity limit (small concentration x) where the elastic properties of both of the pure crystals ($x = 0$ and $x = 1$) are *isotropic* and the same. The influence of different atomic scattering amplitudes on the intensity has also been analysed. Distortions occur in the crystal caused by the size mismatch of the impurity atoms, which results in diffuse scattering of which the most important component is the *Huang* scattering around the Bragg peaks. The Huang scattering has the shape of a *double drop* and we obtain surprisingly good agreement between the continuum and lattice approaches. This is because long-wavelength concentration waves make the dominant contribution to the divergent Huang scattering, with the remainder of the diffuse scattering being very weak. We have also analysed the influence of elastic anisotropy on the diffuse scattering.

1. Introduction

The theory of diffuse scattering from random alloys was developed many years ago. After the very important early work of Huang [1], a rather complete theory of the diffuse scattering from alloys was developed by Krivoglaz and co-workers [2–4] in the Ukraine. This pioneering work contains most of the formalism necessary to understand diffuse scattering in the continuum limit. An English translation of this work is now available and is highly recommended to the interested reader [3]. Of particular interest to us in this paper is the diffuse scattering in a semiconductor caused by a single impurity due to the lattice strain and the associated size mismatch between the impurity and the host.

Modern simulation techniques on lattices allow the individual atomic displacements to be found and hence the associated diffuse x-ray or neutron scattering to be calculated. A crystalline alloy has a mean long-range order that leads to Bragg peaks, and the associated Huang scattering [1] is divergent very close to these Bragg peaks. In this paper we compare the lattice and continuum approaches and find that the continuum approach is remarkably good in all cases. This was anticipated near the Bragg peaks, but in fact the continuum is found to be a good approximation everywhere in the case of small defect concentration. This is because the lattice structure only becomes important at short wavelengths where the diffuse

† Permanent address: National Technical University of Ukraine, Prospekt Pobedy 37, Kiev 56, Ukraine. E-mail address: barabash@amath.pp.kiev.ua.
‡ Permanent address: Department of Physics, Chungbuk National University, Gaeshin-dong, Cheongju-shi, Chungbuk, 361-763, Republic of Korea. E-mail address: chung@phys.chungbuk.ac.kr.
§ E-mail address: thorpe@pa.msu.edu.

0953-8984/99/153075+16$19.50

scattering is very weak anyway. Nevertheless the excellence of the continuum approximation was somewhat of a surprise to us.

In this paper, we first describe the lattice simulations. We look only at the special case of semiconductors with a single defect, where the elastic constants of the host and the defect are isotropic and the same. This is accomplished by using a Kirkwood model [5]. In section 3, we review the continuum approximation for a single defect. In section 4, we compare results for the displacement field around the single defect, and in section 5, we compare the results for the diffuse scattering, using a variety of graphical representations. We analyse diffuse scattering for an *anisotropic* matrix in section 6. We end with a brief discussion.

Throughout this paper we consider only a single defect in a zinc-blende structure. This is the limit at a small concentration x of the alloy $A_{1-x}B_xC$. We use masses that correspond to the alloy $Ga_{1-x}In_xAs$, and force constants in a Kirkwood model, which contains bond-stretching and angle-bending terms, where the force constants are chosen to give the elastic constants of GaAs. This is an initial study, where we have simplified everything, except for the size mismatch between the Ga and In ions which is the crucial ingredient.

2. Lattice simulations

The zinc-blende structure contains two sublattices, each with a face-centred cubic structure. A single impurity is placed in one of these sublattices and the subsequent lattice relaxation and associated diffuse scattering is studied. The direct simulation of the scattering from the atoms in the lattice was based on a numerical procedure [6] which adjusts the positions of all atoms and the size of the cubic supercell to minimize the energy for an alloy $A_{1-x}B_xC$. The size mismatch was described with a Kirkwood potential [5] following the scheme of Thorpe and co-workers [6–9] for an $A_{1-x}B_xC$ semiconductor alloy. The lattice contains two kinds of bond between atoms from the two sublattices, the second sublattice being always occupied by C atoms. The distorted equilibrium structure is obtained by minimizing the energy associated with the Kirkwood potential [5]:

$$V = \frac{\alpha}{2}\sum_{\langle ij\rangle}(L_{ij} - L_{ij}^0)^2 + \frac{\beta}{8}L_e^2\sum_{\langle ijk\rangle}(\cos\theta_{ijk} + \tfrac{1}{3})^2. \tag{1}$$

Here L_{ij} is the length of the bond ij and L_{ij}^0 is the natural (unstrained) bond length L_{ij}^0, which can take on the values L_{AC}^0, L_{BC}^0 with probability $1-x$ and x respectively. The change of this

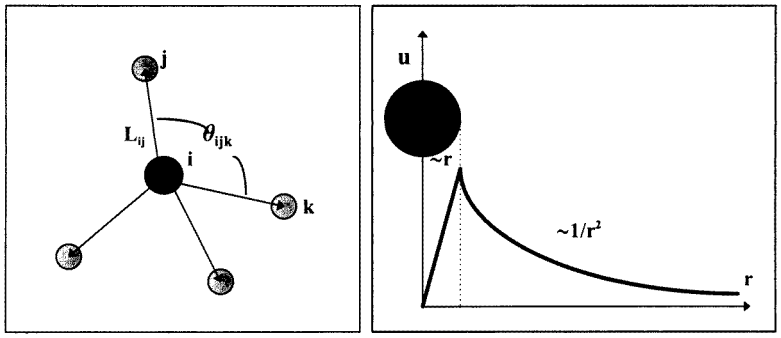

(a) (b)

Figure 1. (a) A sketch of the tetrahedron surrounding the impurity atom in the zinc-blende structure and (b) the radial displacement field around the atom as obtained from the continuum theory.

bond length is related to the stretching force constant α. The angle θ_{ijk} is the variable associated with the tetrahedral angle which has a natural (i.e. unstrained) value of $\cos^{-1}(-1/3) = 109^\circ$. The indices j, k are nearest neighbours to the central atom i as shown in figure 1(a). The change of the angle θ_{ijk} is controlled by the bending force constant β. The mean bond length is L_e and is given in equation (5), below.

In a first-order approximation, consistent with using a harmonic potential (1), the bond length can be written as

$$L_{ij} = L_e + \hat{r}_{ij} \cdot \vec{u}_{ij} \tag{2}$$

where L_e is the nearest-neighbour distance of the undistorted virtual crystal, $\vec{u}_i$ is the displacement of site i from its position in the undistorted structure, and $\vec{u}_{ij} = \vec{u}_j - \vec{u}_i$. The unit vector $\hat{r}_{ij}$ joins sites i, j in the undistorted structure. We will take all of the spring constants to be equal in this paper as it simplifies the analytical treatment [9], and choose the ratio β/α to correspond to *isotropic* elastic constants (which does not qualitatively influence the results). The isotropy condition $c_{11} - c_{12} = 2c_{44}$ for the elastic constants is imposed with the result that the following relations between the elastic moduli and the force constants [9]

$$c_{11} = \frac{1}{3a}\left(\alpha + 3\beta - \frac{\lambda}{3}\beta\right) \qquad \text{and} \qquad c_{12} = \frac{1}{3a}\left(\alpha - \beta - \frac{\lambda}{3}\beta\right) \tag{3}$$

reduce to $\alpha = 16\beta/9$ for the Kirkwood model where $\lambda = 1$ [5] ($\lambda = 0$ for the Keating model [10], which we do not use here). For isotropic elastic moduli in crystalline $Ga_{1-x}In_xAs$, we used the following values of the force constants: $\alpha = 49.138$ N m^{-1}; $\beta = 27.64$ N m^{-1}, leading to the elastic moduli $c_{11} = 7.2432$ dyn cm^{-2} with $c_{12} = c_{11}/10$, and hence the Poisson ratio $\nu = 2c_{12}/c_{11} = 0.2$. The unstrained length of the GaAs bond is $a_2 = 2.4479$ Å and that of the InAs bond is $a_1 = 2.6233$ Å. The mismatch in length of the InAs bond compared with the GaAs bond is about 7%.

The scattering intensity was computed from the relaxed coordinates using the expression [11]

$$I(\vec{Q}) = \left| \sum_i f_i \exp(\mathrm{i}\vec{Q} \cdot \vec{R}_i) \right|^2 \tag{4}$$

where $I(\vec{Q})$ is the total scattering intensity, and $\vec{Q}$ is the diffraction vector, $\vec{Q} = \vec{k}_1 - \vec{k}_0$. The wavevectors $\vec{k}_1$ and $\vec{k}_0$ are associated with the scattered and incident beams, respectively, with $|\vec{k}_1| = |\vec{k}_0| = 2\pi/\lambda$, where λ is the x-ray or neutron wavelength. We also will use the quantity $\vec{q} = \vec{Q} - \vec{G}$ to describe the scattering around a single reciprocal-lattice vector $\vec{G}$. The factor f_i is the strength of the scattering from an individual atom i, and is the atomic form factor for x-ray scattering (which is proportional to the atomic charge Z at small wavevector $\vec{Q}$) and the neutron scattering length for neutron scattering.

For a direct computer simulation of the scattering intensity of random semiconductor alloys with the zinc-blende structure, we used a supercell with $L \times L \times L$ cubes of the zinc-blende structure, each containing eight atoms, with periodic boundary conditions. A single impurity atom was placed in this large supercell. Different supercell sizes were tested for direct simulations over the lattice to evaluate the influence of the size of the supercell on the accuracy of the calculation of the displacement field and diffuse scattering intensity, and in order to obtain a denser mesh of points for the calculation of the diffuse scattering. The simulation program, which used a variant of the conjugate gradient method [6], adjusted the positions of all atoms at a given size of the supercell to minimize the energy. The simulation was terminated when the strain energy did not change within ten significant digits. It was found that $L = 40$, which corresponds to 512 000 atoms in the supercell, was large enough, and this value is used

throughout this paper. The supercell was kept strictly cubic and its size scaled by the mean bond length as required by Vegard's law, which is known to hold strictly for the conditions here (no force constant disorder [9]). The mean bond length [9] is given by Vegard's law [12]

$$L_e = (1-x)L^0_{\mathrm{AC}} + xL^0_{\mathrm{BC}}. \tag{5}$$

Although the defect concentration $x = 1/256\,000$ is very small in this calculation, it is important to make this adjustment to the sample size, using (5), as the diffuse scattering is only meaningful at the superlattice points in reciprocal space associated with the supercell, and we found that it was important to be *exactly* at these points. Note that we use the full expression (4) for the scattered intensity with these lattice calculations and make no assumptions about small displacements and expanding the expression (4) as is done in the continuum theory.

3. Continuum theory

The continuum theory of diffuse scattering from isolated defects [2–5, 13–16] gives a detailed analysis of isodiffuse surfaces in the vicinity of reciprocal-lattice sites for cubic crystals. This theory has been worked out for a wide variety of geometries and defect types and is summarized in a recent book [3]. We will present here a simple derivation of the isotropic case of interest to us in this paper.

Consider an elastic sphere with radius R_1, subject to an external hydrostatic pressure P_1. The displacement $\vec{u}_1$ is only in the radial direction inside the sphere, is linear in r, and can be easily calculated using continuum mechanics [17] as

$$\vec{u}_1 = -\frac{P_1}{3K}\vec{r} \tag{6}$$

where K is the bulk modulus of the material. We now consider the *inverse* situation, of an infinite elastic continuum, containing a spherical hole of size R_2, with an inside hydrostatic pressure P_2. In this case the displacement field $\vec{u}_2$ is also radial and is given by an inverse square behaviour with distance

$$\vec{u}_2 = \frac{P_2 R_2^3}{2\mu r^2}\hat{r} \tag{7}$$

where $\hat{r}$ is a unit vector along $\vec{r}$. We assume that $R_1 > R_2$, and put the *larger sphere* inside the *smaller spherical hole*. The boundary conditions are that the pressure is continuous and the radial displacement field is continuous. These two conditions lead to the pressure at the boundary:

$$P = P_1 = P_2 = \frac{R_1 - R_2}{R_2/4\mu + R_1/3K}. \tag{8}$$

Of most interest to us here is how the displacement field falls off outside the impurity, and this is given by

$$\vec{u}_2 = \frac{R_1 - R_2}{R_2/4\mu + R_1/3K}\frac{R_2^3}{2\mu r^2}\hat{r}. \tag{9}$$

Note that the bulk modulus K is associated with the *inner* material and the shear modulus μ with the *outer* material, although here we do not make any distinction as the two materials are assumed to be the same elastically. We can rewrite the result (9) in a more convenient form if we use the fact that the difference $\Delta R = R_1 - R_2$ is small, and also use the Poisson ratio ν as given by $K/\mu = \frac{2}{3}(1+\nu)/(1-2\nu)$ so that (9) becomes

$$\vec{u}_2 = \frac{\Delta R}{3R}\left(\frac{1+\nu}{1-\nu}\right)\frac{R^3}{r^2}\hat{r} = \frac{\Delta V}{12\pi r^2}\left(\frac{1+\nu}{1-\nu}\right)\hat{r} \tag{10}$$

which depends only on two parameters: the change in volume ΔV associated with the mismatch, and the Poisson ratio ν. A sketch of this displacement field around the impurity is shown in figure 1(b), which shows the $1/r^2$ behaviour outside the sphere.

The scattering amplitude can be found from the Fourier transform $\vec{u}_{\vec{q}}$ of the displacement field. We neglect the displacement field $\vec{u}_1$ inside the sphere, and calculate $\vec{u}_{\vec{q}}$ as

$$\vec{u}_{\vec{q}} = \int \vec{u}_2 \exp(\mathrm{i}\vec{q}\cdot\vec{r})\,\mathrm{d}^3r/V_a = \mathrm{i}\frac{\Delta V}{V_a}\frac{\hat{q}}{q}\frac{(1+\nu)}{3(1-\nu)} \tag{11}$$

where V_a is the volume per atom (i.e. the volume of the sample divided by the total number of atoms including both sublattices). The expression above is only meaningful for small wavevectors $\vec{q}$ as we are in the continuum limit.

The expression for the scattered intensity (4) can be rewritten using the equilibrium positions in the virtual crystal $\vec{R}_i^0$, where $\vec{R}_i = \vec{R}_i^0 + \vec{u}_i$, as

$$\begin{aligned} I(\vec{Q}) &= \left| f\sum_i \exp(\mathrm{i}\vec{Q}\cdot\vec{R}_i^0)\exp(\mathrm{i}\vec{Q}\cdot\vec{u}_i)\right|^2 = \left| f\sum_i \exp(\mathrm{i}\vec{Q}\cdot\vec{R}_i^0)[1+\mathrm{i}\vec{Q}\cdot\vec{u}_i]\right|^2 \\ &= \left| f\sum_i \exp(\mathrm{i}\vec{Q}\cdot\vec{R}_i^0)\right|^2 + |f\vec{Q}\cdot\vec{u}_{\vec{q}}|^2 = I_B(\vec{Q}) + I_H(\vec{Q}) \end{aligned} \tag{12}$$

where we have set all of the amplitude factors f_i in equation (4) equal to f for simplicity. The first term in (12) is the Bragg scattering $I_B(\vec{Q})$ associated with the virtual crystal and the second term is the Huang scattering $I_H(\vec{Q})$, where we have taken only the leading non-zero term in (12) which is dominant. Note that the wavevector $\vec{q}$ is associated with each reciprocal-lattice vector in turn via $\vec{q} = \vec{Q} - \vec{G}$. Using equations (11) and (12), the Huang scattering in the continuum limit is

$$I_H(\vec{Q}) = \left[f\left(\frac{\Delta V}{V_a}\right)\left(\frac{1+\nu}{3(1-\nu)}\right)\left(\frac{\vec{Q}\cdot\hat{q}}{q}\right)\right]^2 \tag{13}$$

for a single defect. In the low-concentration limit, the scattering from isolated defects will be additive, and so the above expression would just be multiplied by the number of defect atoms to get the total scattering. Note that the first factor in (13) is the relative size change associated with the impurity atom where $\Delta V/V_a = 3\,\Delta R/R$. Note also that this is the change in the *natural length* associated with the substitution of a host atom with an impurity and not the *actual length change*, which in general will be smaller in magnitude, because of the restraining effect of the rest of the lattice.

For a small concentration of defects in an elastically isotropic medium in the vicinity of reciprocal-lattice sites, classic Huang scattering occurs as found by many previous authors [2–4, 13–16] whose result we reproduce here:

$$I_H(\vec{Q}) = N_d|f|^2\mathrm{e}^{-2W}\left(\frac{1}{V_t}\frac{\mathrm{d}V_t}{\mathrm{d}x}\right)^2\left(\frac{1+\nu}{3(1-\nu)}\right)^2\frac{Q^2\cos^2\theta}{q^2} \tag{14}$$

which is proportional to $\cos^2\theta$, where θ is the angle between $\vec{Q}$ and $\vec{q}$. This results in the appearance of strong Huang scattering around *all* reciprocal-lattice points having the shape of a *double drop*. In expression (14), N_d is the number of defects and f is an average scattering factor that has been put back. The Debye–Waller factor involving W can be ignored for a single defect as it is a $1/N$ effect, where N is the total number of atoms. The quantity V_t is the total volume of the crystal and so using Vegard's law (5), we see that equation (14) does indeed reduce to (13) in the appropriate limit as expected, including the overall normalization. We have found the simple calculation of Huang scattering given in this section instructive, and perhaps simpler than some of the traditional calculations that have led to (14).

In the case when all of the scattering factors f_i in (4) are *not* all set equal, the separation into Bragg and Huang scattering in (12) must be done with more care [2–4]. In particular there are the strong Bragg peaks that we have been discussing, with their associated diffuse scattering $I_D(\vec{Q})$ given by

$$I_D(\vec{Q}) = \left[\frac{(f_A + f_C)}{2}\left(\frac{\Delta V}{V_a}\right)\left(\frac{1+\nu}{3(1-\nu)}\right)\left(\frac{\vec{Q}\cdot\hat{q}}{q}\right) + (f_A - f_B)\right]^2 \tag{15}$$

where the diffuse scattering $I_D(\vec{Q})$ becomes the Huang scattering $I_H(\vec{Q})$ as given in (12) and (13) when all of the atomic scattering factors f_i are set equal. In general the diffuse scattering in (15) contains the divergent Huang amplitude and another non-divergent amplitude, which increases the scattering slightly on one side of the peak and decreases it on the other.

When $f_A \neq f_C$ additional Bragg peaks occur. These are the extra peaks that are observed in the zinc-blende structure but not seen in the diamond structure. There is diffuse scattering associated with these weak peaks also, which has the form

$$I_D(\vec{Q}) = \left[\frac{(f_A - f_C)}{2}\left(\frac{\Delta V}{V_a}\right)\left(\frac{1+\nu}{3(1-\nu)}\right)\left(\frac{\vec{Q}\cdot\hat{q}}{q}\right) + (f_A - f_B)\right]^2 \tag{16}$$

and disappears completely when all the scattering factors are set equal to unity. Note that the diffuse scattering in (15) is associated with strong Bragg peaks whose intensity scales as $(f_A + f_C)^2$, whereas the diffuse scattering in (16) is associated with weaker Bragg peaks whose intensity scales as $(f_A - f_C)^2$. The Huang part of the diffuse scattering scales quadratically with the atomic form factor in the same way as the Bragg peak with which it is associated. So if one is strong so is the other, and vice versa.

4. Displacement field

For defects in an elastically isotropic medium, the substitution for the host atom with an impurity atom is accompanied by the action of hydrostatic pressure on the surface of the impurity atom due to the size mismatch of host and impurity atoms, in the continuum viewpoint. This results in the appearance of an inverse-square-type displacement field in the matrix as sketched in figure 1(b) decreasing as $1/r^2$ with the distance r between the defect and the matrix site, as discussed in the previous section.

There is a question as to the proper choice of the length change ΔR or equivalently the volume change ΔV associated with the defect that should be used in equation (10). This forms the *bridge* between the continuum theory and the lattice simulations. One possible choice would be to take the volume associated with the GaAs bond length a_2 as $4\pi a_2^3/3$ so that

$$\Delta V = 4\pi(a_1^3 - a_2^3)/3 = 14.2\ \text{Å}^3.$$

This was too large when compared with simulations results.

The proper procedure [2, 3] is to take the Wigner–Seitz cell surrounding the Ga ion, and ignoring the As ions, to give a volume of $16a_2^3/3\sqrt{3}$, and hence

$$\Delta V = 16(a_1^3 - a_2^3)/3\sqrt{3} = 10.4\ \text{Å}^3$$

which gives a better fit to the lattice simulation data. Actually the best fit was obtained with the linearized version of this result

$$\Delta V = 16a_2^2(a_1 - a_2)/\sqrt{3} = 9.71\ \text{Å}^3$$

which is what we use in equation (10) and is shown as the curves in figures 2(a) and 3.

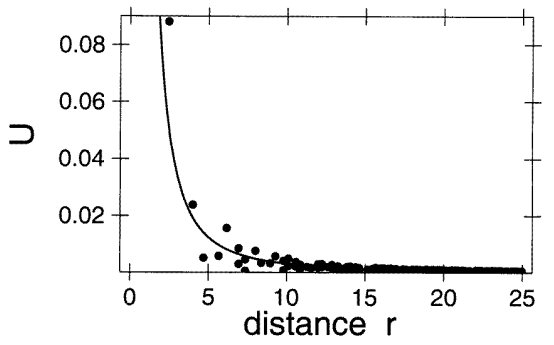

(a)

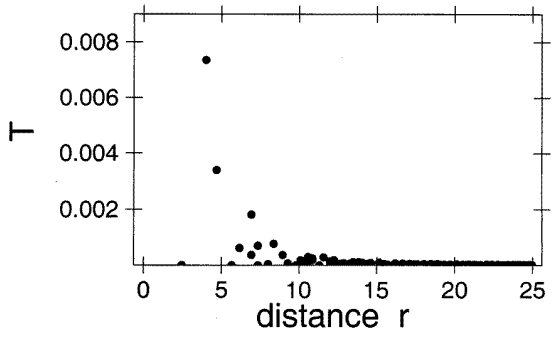

(b)

Figure 2. Showing (a) the radial $U = \vec{u} \cdot \hat{r}$ and (b) the tangential $T = |\vec{u} \times \hat{r}|$ parts of the displacement field calculated by direct simulation over the lattice (solid dots) and calculated from the continuum theory given in equation (10) for a single defect using the continuum approach (curve). Note that the tangential displacements are ten times smaller and predicted to be zero by the continuum theory. The distance r is measured in ångströms.

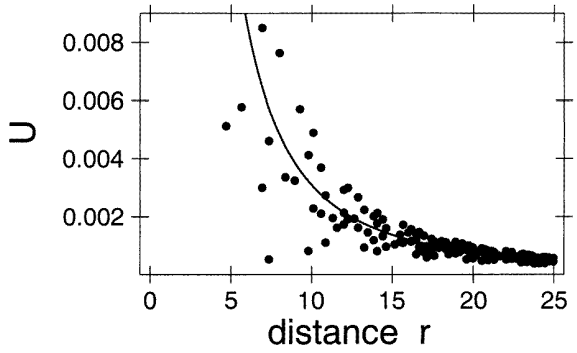

Figure 3. Showing an enlargement from figure 2(a) of the radial $U = \vec{u} \cdot \hat{r}$ part of the displacement field calculated by direct simulation over the lattice (solid dots) and calculated from the continuum theory given in equation (10) for a single defect using the continuum approach (curve). The distance r is measured in ångströms.

To check the displacement field caused by In atoms in a GaAs matrix with the ratio between bond-bending and bond-stretching force constants β/α corresponding to an isotropic

elastic medium, we have simulated the displacement field for such a crystal with one In atom substituted for a Ga atom in a sample size of $40 \times 40 \times 40$ cells with 512 000 atoms. The changes of the radial and tangential parts of the displacement field with the distance from the impurity atoms are shown in figures 2(a) and 2(b). We have verified that the displacement field falls off as an *inverse square* law at large distances from the single defect as predicted by continuum theory, but that there are significant deviations *close* to the defect. The theoretical curve corresponding to equation (10) is shown by a solid curve, the results of simulations are represented by dots. In figure 3, we show an enlargement of figure 2(a) which shows that there are small but real fluctuations away from the inverse square behaviour at all distances.

It is seen that the tangential part of the displacement field is *ten times smaller* than the radial component, so we can use this approximation and consider the displacement field created by In impurity atoms as being of an inverse square type. The deviation of the displacement field from a pure inverse square behaviour in the several nearest neighbours will influence the intensity distribution at large distances from the reciprocal-lattice points, while in the vicinity of a reciprocal-lattice point, the scattered intensity is caused mainly by the atoms relatively distant from the defect (where the inverse square type of displacement field is good, on average).

The deviations from the inverse square law shown in figure 2(a) and 3 are real and not due to any numerical noise or error, as we have checked this with different supercell sizes, and obtained identical results. These deviations appear to cancel out in the Huang scattering almost completely, as seen in the next section.

5. Diffuse scattering

In this section, we give results for the diffuse scattering associated with a single In defect in a GaAs host, with all the force constants α and β the same and chosen to give isotropic elastic behaviour as described previously. All of the lattice simulations are over a 512 000-atom supercell and the continuum calculations have been described in section 3.

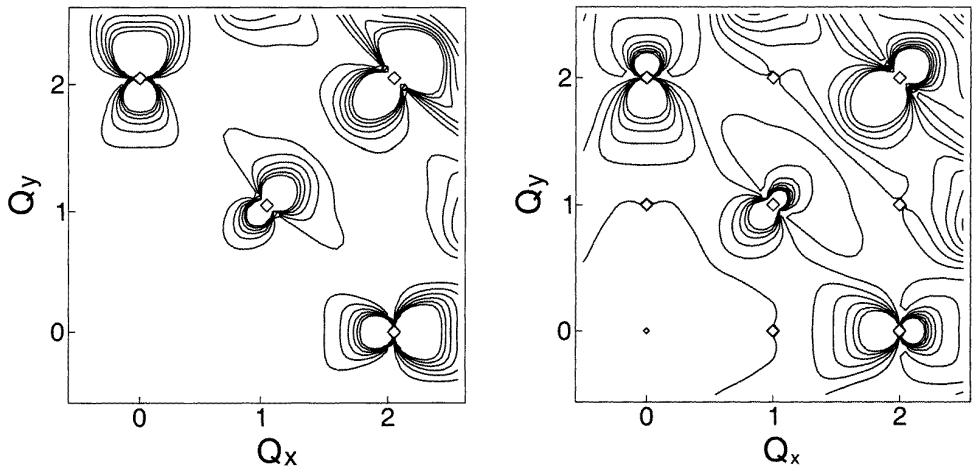

Figure 4. Contour maps of the diffuse scattering, from lattice simulations, for a single In defect in GaAs with isotropic elastic properties. In (a) the contours are for equal scattering amplitudes $f_A = f_B = f_C = 1$ and in (b) they are for different scattering amplitudes $f_A = 31$, $f_B = 49$, and $f_C = 33$.

Again we must select the appropriate value of the relative volume change $\Delta V/V_a$ for use in equation (13). From the previous discussion, this is associated with the change in the natural bond lengths of InAs and GaAs and hence $\Delta V/V_a = (a_1/a_2)^3 - 1 = 0.231$. As before we find that the linear result, $\Delta V/V_a = 3[(a_1/a_2) - 1] = 0.215$, gives a slightly better fit when used in equation (13) to fit the lattice simulations of the diffuse scattering as shown in figure 4 (and figures 6 and 7—see later).

To get an overview of the scattering, we show in figure 4 a contour map of curves of equal intensity for the diffuse scattering. These were calculated from the lattice simulation, using the

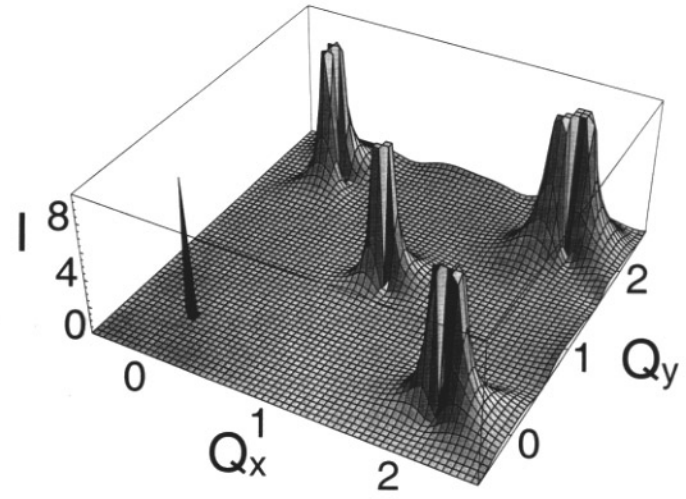

(a)

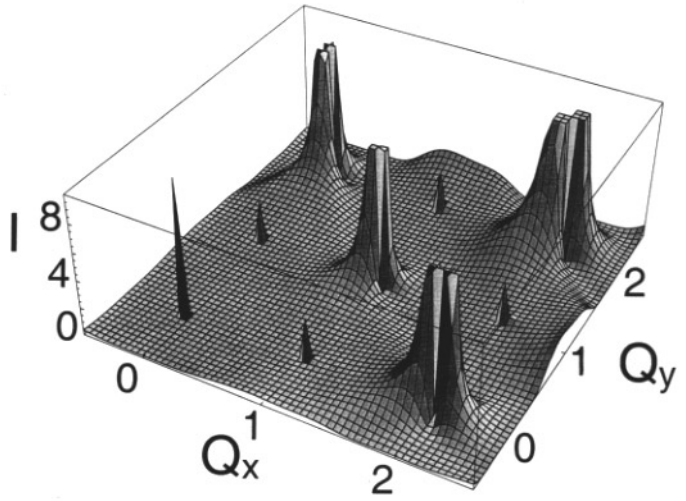

(b)

Figure 5. Showing the spatial distribution of the total scattered intensity, I, from the lattice simulations, for a single In defect in GaAs with isotropic elastic constants with (a) equal scattering amplitudes $f_A = f_B = f_C = 1$ and (b) different scattering amplitudes $f_A = 31$, $f_B = 49$, and $f_C = 33$. The intensity is normalized to $(f_A + f_C)^2/4$.

relaxed atomic coordinates and equation (4). These contours are calculated for the (001) plane ($q_z = 0$) for the case in which the change in scattering amplitude is neglected ($\Delta f = 0$) (a) and for different scattering amplitudes with $\Delta f \neq 0$ (b). The *double-drop* shapes around the (200), (020), (110), and (220) reciprocal-lattice points are aligned so that the axes point *towards* the origin. Slight anisotropy of the contours is caused by $\vec{Q}$ being larger on the distant side of the reflection. It can be seen from figure 4(b) that the difference of scattering amplitudes switches the anisotropy of the intensity distributions in the vicinity of reciprocal-lattice points, while at large distances the scattering is almost the same. Notice that the smaller Bragg peaks that scale as $(f_A - f_C)^2$ together with their associated Huang scattering are just visible in figure 4(b). The wavevector $\vec{Q}$ is in units of $4\pi/a_2$ in figures 4–10.

In figure 5 we show a different representation of the same results as in figure 4, but also include the Bragg peaks this time. It can be seen that additional smaller Bragg peaks occur when the scattering amplitudes are not the same, as this corresponds to the difference between the zinc-blende and diamond structures. In particular, we see the appearance of additional Bragg

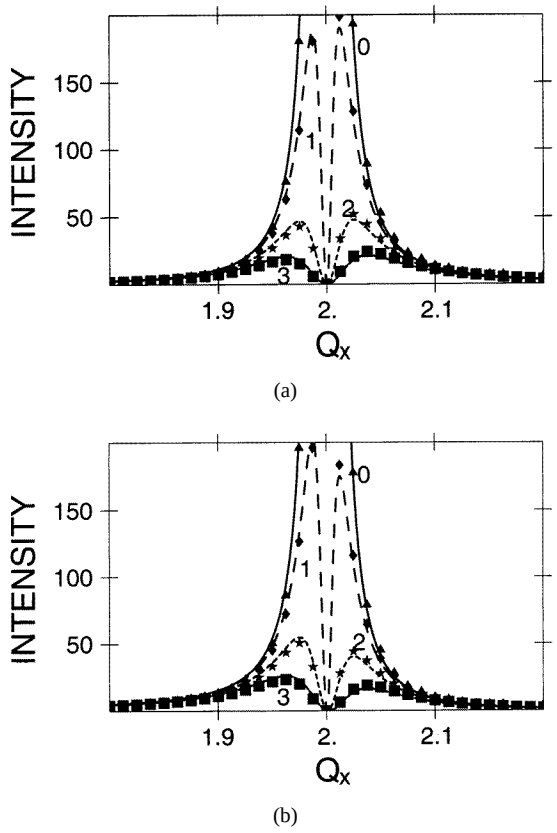

Figure 6. Showing the profile of the Huang scattering intensity from a single In defect in GaAs with isotropic elastic constants, for the (200) reflection along the [100] direction for different values of q_y which is perpendicular to the x-direction. The curves are from the continuum theory and the corresponding symbols are from the lattice simulation. The values of q_y are (0) 0, (1) $0.0125G$, (2) $0.025G$, and (3) $0.0375G$, where $G = 4\pi/a$, and the nearest-neighbour bond length is $\sqrt{3}a_2/4$. The top panel (a) shows the case for equal scattering $f_A = f_B = f_C = 1$, and the bottom panel (b) that for different scattering amplitudes $f_A = 31$, $f_B = 49$, and $f_C = 33$. The intensity is normalized to $(f_A + f_C)^2/4$.

peaks in the positions corresponding to the reflections (100), (010), (210), (120). Notice that the Huang scattering around the large peaks in figure 5(b) is substantial as predicted by (15) and extremely weak around the smaller Bragg peaks as predicted by (16).

In figure 6, we show the results of the direct lattice simulations (solid symbols) and the continuum result (curves) for the (200) strong Bragg reflection for different values of q_y along the direction [100], which show remarkably good agreement with each other, not only for the section passing through the centre of the reflection but also for a section passing through the side parts of it. We observe the decrease of the intensity in the central part of these distributions for a side section typical for the *double-drop* shape of the reflection. The anisotropy of the profiles is different for the case (a) with $\Delta f = 0$ and compared with equation (14), and the case (b) with $\Delta f \neq 0$ and compared with equation (15). The short-wavelength concentration waves, that are very different in the lattice and continuum theories, are only important when the scattering is weak out in the wings of the Huang scattering, and so in fact are seen to be largely irrelevant. Nevertheless it was not clear to us before doing this study that the continuum approach would be so spectacularly good.

In figure 7, we show that the Huang scattering increases as the scattering vector $\vec{Q}$ increases in a quadratic way as Q^2 for *both* the strong and weak series of Bragg peaks separately. The diffuse scattering associated with the strong Bragg peaks is compared to the continuum theory in equation (15) and that associated with the weak Bragg peaks is compared to the continuum theory in equation (16).

The agreement of the lattice simulations with the continuum approximation is very good in all cases. Finally in figure 8, we show an enlarged picture of the diffuse scattering associated with one of the weak Bragg peaks in figure 7, which shows some small deviations from the continuum theory. This is not unexpected as the scattering is very weak and continuum theory is after all only an approximation to the lattice.

The second non-divergent terms in equations (15) and (16) do have small but observable effects on the intensity in the wings of the Huang scattering as can be seen in figures 4–8. These terms can be thought of as providing a background scattering everywhere. However, because they add as amplitudes and not as intensities, they can cause an asymmetry in the wings of the Huang scattering as shown for example in figure 8.

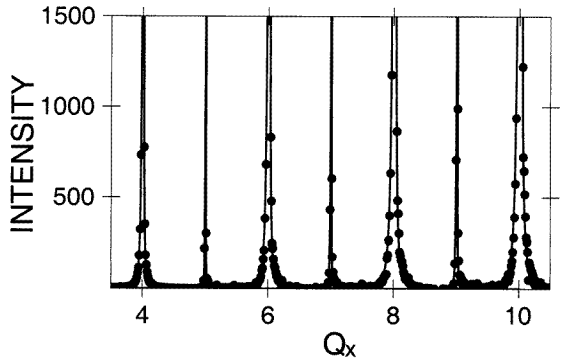

Figure 7. A panoramic view of the diffuse intensity profile along direction [100] for higher orders of the reflection (200) for a single In defect in GaAs with isotropic elastic constants and scattering amplitudes $f_A = 31$, $f_B = 49$, and $f_C = 50$. We have made f_C larger to emphasize the diffuse scattering around the smaller peaks. The curves are from the continuum theory and the solid circles are from the lattice simulation. The intensity is normalized to $(f_A + f_C)^2/4$. The curves alternate: strong, weak, ...

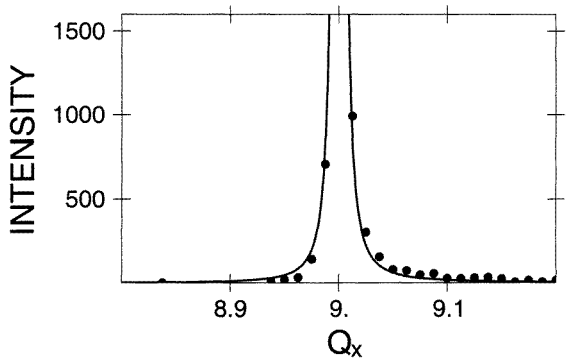

Figure 8. An expanded view of the diffuse scattering associated with one of the weak Bragg peaks in figure 7. The intensity is normalized to $(f_A + f_C)^2/4$.

6. Cubic elastic constants

Real crystals are not isotropic. The extent of the matrix anisotropy for cubic crystals can be characterized with the anisotropy parameter $\xi = (c_{11} - c_{12} - 2c_{44})/c_{44}$ depending on the elastic moduli c_{11}, c_{12}, and c_{44}. For an isotropic medium, $\xi = 0$. Anisotropy parameters ξ of semiconductors with the zinc-blende structure are shown in the table 1. It can be seen that most have a *negative* anisotropy parameter in the interval $-0.6 > \xi > -1.2$. For the Kirkwood model, the anisotropy parameter is given by $\xi = (16/9)(\beta/\alpha) - 1$, depending only on the *ratio* β/α. The parameters α and β determined from c_{11} and c_{12} in the Kirkwood model give a slightly different value of c_{44}, for GaAs, and take the anisotropy parameter ξ different from -1 which would correspond to $\beta = 0$. Note that values of the anisotropy parameter $\xi < -1$ are not attainable in the Kirkwood model, which may be a significant deficiency, especially in the present study where the Huang scattering is dominated by long wavelengths and hence depends almost exclusively on the elastic constants. However, as our aim in this paper is to check the continuum approximation for a given set of elastic constants, rather than to describe real materials accurately, this is not much of a concern here.

The parameters used in the continuum calculations are $c_{11} = 11.9$, $c_{12} = 5.38$, $c_{44} = 4.712$ (in units of 10^{11} dyn cm^{-2}) which corresponds to an anisotropy parameter $\xi = -0.616$, with force constants $\alpha = 128.1$ N m^{-1}, $\beta = 27.64$ N m^{-1} which gives the ratio $\beta/\alpha = 0.216$. The force constant parameters α, β were calculated from the elastic moduli c_{11} and c_{12}. The absolute value of these force constants is not important, rather only the ratio β/α or equivalently the anisotropy parameter ξ.

Matrix anisotropy changes the continuum equation for Huang scattering intensity. It is additionally influenced by elastic constants and the value of the anisotropy parameter ξ for the matrix. For a single defect in the case in which all of the amplitude factors f_i in (4) are equal to unity, the Huang scattering intensity (13) becomes

$$I_H(\vec{Q}) = \left(\frac{\Delta V}{V_a}\right)^2 \left(\frac{c_{11} + 2c_{12}}{3D(\hat{n})}\right)^2 \frac{Q^2}{q^2} A^2(\hat{m}, \hat{n}) \tag{17}$$

where $\hat{m} = \vec{Q}/Q$, $\hat{n} = \vec{q}/q$, and

$$A(\hat{m}, \hat{n}) = m_x n_x (1 + \xi n_y^2)(1 + \xi n_z^2) + m_y n_y (1 + \xi n_z^2)(1 + \xi n_x^2) + m_z n_z (1 + \xi n_x^2)(1 + \xi n_y^2) \tag{18}$$

$$D(\hat{n}) = c_{11} + \xi(c_{11} + c_{12})(n_x^2 n_y^2 + n_x^2 n_z^2 + n_y^2 n_z^2) + \xi^2 (c_{11} + 2c_{12} + c_{44}) n_x^2 n_y^2 n_z^2. \tag{19}$$

Table 1. The elastic constants c_{11}, c_{12}, and c_{44} (in units of 10^{11} dyn cm^{-2}) from reference [18] and the dimensionless anisotropy parameter ξ are listed for crystals with the diamond and zinc-blende structures. The force constants α and β (in N m^{-1}) for the Kirkwood model are also given.

	c_{11}	c_{12}	c_{44}	ξ	α	β
Diamond structure						
C	10.76	1.25	5.77	−0.35	47.3	25.5
Si	16.58	5.78	8.00	−0.65	153.0	44.0
Ge	12.85	4.83	6.68	−0.80	127.3	34.1
Zinc-blende structure						
AlP	14.59	6.71	3.69	+ 0.14	153.0	32.3
	18.83	8.44	4.24	+ 0.45	195.1	42.6
AlAs	12.02	5.70	5.8	−0.93	132.6	26.8
AlSb	8.77	4.34	4.08	−0.91	107.1	20.4
GaP	14.05	6.20	7.03	−0.88	144.2	32.1
GaAs	11.90	5.38	5.95	−0.90	128.1	27.6
GaSb	8.83	4.02	4.32	−0.89	102.9	22.0
InP	10.11	5.61	4.56	−1.01	125.2	19.8
InAs	8.33	4.53	3.96	−1.04	105.3	17.3
InSb	6.67	3.65	3.02	−1.00	90.5	14.7
ZnS	9.81	6.27	4.48	−1.21	120.9	14.4
ZnSe	8.59	5.06	4.06	−1.13	106.0	15.0
ZnTe	7.13	4.07	3.12	−1.02	93.20	14.0
CdS	8.47	5.45	1.58	−0.09	112.7	13.2
CdSe	7.49	4.61	1.32	+ 0.19	101.1	13.1
CdTe	5.33	3.65	2.04	−1.18	81.9	8.17
HgSe	6.19	4.42	2.23	−1.20	91.5	8.08
HgTe	5.36	3.66	2.12	−1.20	81.9	8.24

In the case in which the scattering factors f_i in (4) are *not* all set equal, the intensity of the diffuse scattering associated with main Bragg peaks (15) is given by

$$I_D(\vec{Q}) = \left[\frac{(f_A + f_C)}{2}\left(\frac{\Delta V}{V_a}\right)\left(\frac{c_{11} + 2c_{12}}{3D(\hat{n})}\right)\left(\frac{Q}{q}\right)A(\hat{m},\hat{n}) + (f_A - f_B)\right]^2. \tag{20}$$

As in the case of isotropic elastic constants, the latter becomes the Huang scattering $I_H(\vec{Q})$ as given in (17) when all of the atomic scattering factors f_i are set equal to unity. The diffuse scattering intensity around the additional extra peaks (16) related to the non-zero difference between the A and C atomic scattering factors $f_A \neq f_C$ in the case of cubic lattice constants of the matrix now is described by

$$I_D(\vec{Q}) = \left[\frac{(f_A - f_C)}{2}\left(\frac{\Delta V}{V_a}\right)\left(\frac{c_{11} + 2c_{12}}{3D(\hat{n})}\right)\left(\frac{Q}{q}\right)A(\hat{m},\hat{n}) + (f_A - f_B)\right]^2. \tag{21}$$

Matrix anisotropy changes the shape of isodiffuse curves from simple spheres to a more complicated shape, while still maintaining the characteristic *double-drop* shape. Contour maps for this case are analogous to those shown in figure 4, but we observe small changes in the shape of the isodiffuse curves. In figures 9(a) and 9(b), we show the results of the direct lattice simulations and the continuum calculation for the (200) strong Bragg reflection for different sections along the [100] direction. These profiles are analogous to those shown in figure 6. The intensity of the diffuse scattering is higher than in the isotropic case, but still the results of simulation and from continuum theory described by equations (17)–(21) again show

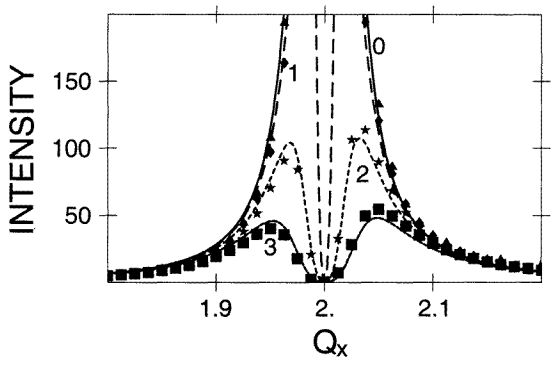

(a)

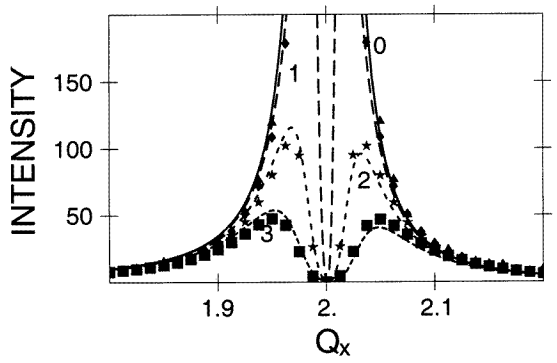

(b)

Figure 9. Showing the profile of the Huang scattering intensity from a single In defect in GaAs with *cubic* elastic constants $c_{11} = 11.9$, $c_{12} = 5.38$, $c_{44} = 4.71$ (in units of 10^{11} dyn cm^{-2}), $\alpha = 128.1$ N m^{-1}, $\beta = 27.64$ N m^{-1}, $\beta/\alpha = 0.216$, $\xi = -0.616$, for the (200) reflection along the [100] direction for different values of q_y which is perpendicular to the x-direction. The curves are from the continuum theory and the corresponding symbols are from the lattice simulation. The values of q_y are (0) 0, (1) $0.0125G$, (2) $0.025G$, and (3) $0.0375G$, where $G = 4\pi/a_2$, and the nearest-neighbour bond length is $\sqrt{3}a_2/4$. The top panel (a) shows the case for equal scattering $f_A = f_B = f_C = 1$, and the bottom panel (b) that for different scattering amplitudes $f_A = 31$, $f_B = 49$, and $f_C = 33$. The intensity is normalized to $(f_A + f_C)^2/4$.

remarkably good agreement with each other. We also checked the coincidence of continuum and lattice simulation results for additional weak peaks (figure 10). It is not quite so good, but still very satisfactory.

7. Discussion

The presence of isolated defects in a semiconductor crystal results in the appearance of intensive Huang scattering around the reciprocal-lattice points. The intensity distribution of Huang scattering for defects in these cubic crystals, with isotropic elastic constants, behaves as $(\vec{Q} \cdot \vec{q})^2/q^4$, where $\vec{Q}$ is the scattering wavevector and $\vec{q} = \vec{Q} - \vec{G}$ is measured from the reciprocal-lattice point $\vec{G}$ of interest. The diffuse scattering is dominated by the Huang component and results in the *double-drop* shape of the isodiffuse surfaces. Results of a *continuum* theory of Huang scattering in the limit of very low concentration coincide with

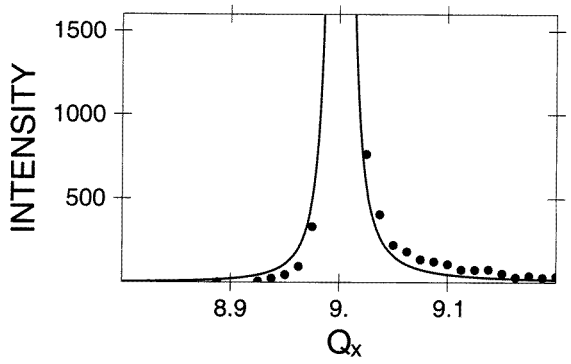

Figure 10. An expanded view of the diffuse scattering associated with one of the weak Bragg peaks for crystals with cubic elastic constants $c_{11} = 11.9$, $c_{12} = 5.38$, $c_{44} = 4.712$ (in units of 10^{11} dyn cm^{-2}), $\alpha = 128.1$ N m^{-1}, $\beta = 27.64$ N m^{-1}, $\beta/\alpha = 0.216$, $\xi = -0.616$. The intensity is normalized to $(f_A + f_C)^2/4$.

those for a relaxed *lattice* model studied here. Huang scattering is expected to be dominated by long wavelengths near the peaks in the scattering, so continuum theory should provide a good description of the scattered intensity. We show that the strong, weak Bragg peaks have strong, weak diffuse scattering associated with them. Matrix anisotropy changes the shape of the isodiffuse curves from simple spheres to more complicated forms, but the *double-drop* characteristic is still retained.

It is a bit of a surprise that continuum theory also does rather well in the wings of the Huang scattering, where shorter wavelengths are important, but this is because the scattering is very weak and featureless. The displacement field associated with a single defect does fall off as an inverse square law on average, but with some deviations about the average due to the lattice structure. As we have shown, there is a very good agreement between lattice and continuum results, and it will be possible now to use continuum theory for calculations of diffuse scattering with considerable confidence. This is the first of a series of studies that we are undertaking to evaluate the continuum approximation to diffuse x-ray and neutron scattering in semiconductor alloys. Future work will consider higher concentrations of defects and the effects of differences in the force constants between the host and the impurities.

Acknowledgments

This work was supported by the US Department of Energy under contract DE-FG02-97ER45651. JSC acknowledges support from the basic Science Research Programme (BSRI-97-2436), Korean Ministry of Education, and RIB acknowledges support from the NSF through a Soros grant (APU072005). A preliminary account of this work is to be published in the proceedings of the European Crystallographic Meeting. Two of us (RIB and JSC) would like to thank the Physics and Astronomy Department at Michigan State University for their hospitality during extended visits. We should like to thank Simon Billinge and Iwona Jasiuk for useful discussions.

References

[1] Huang K 1947 *Proc. R. Soc.* A **190** 102
[2] Barabash R I and Krivoglaz M A 1979 *Phys. Met.* **1** 33

[3] Krivoglaz M A 1996 *The Theory of X-ray and Thermal Neutron Scattering from Real Crystals* (New York: Plenum)
[4] Barabash R I 1997 *Local Structure from Diffraction* ed S J L Billinge and M F Thorpe (New York: Plenum) p 233
[5] Kirkwood J G 1939 *J. Chem. Phys.* **7** 506
[6] Chung J S and Thorpe M F 1997 *Phys. Rev.* B **55** 1545
[7] Thorpe M F and Garboczi E J 1990 *Phys. Rev.* B **42** 8405
[8] Thorpe M F, Chung J S and Cai Y 1991 *Phys. Rev.* B **43** 8283
[9] Cai Y and Thorpe M F 1992 *Phys. Rev.* B **46** 15 872
Cai Y and Thorpe M F 1992 *Phys. Rev.* B **46** 15 879
[10] Keating P N 1966 *Phys. Rev.* **145** 637
[11] Lovesey S W 1984 *Theory of Neutron Scattering from Condensed Matter* (Oxford: Clarendon)
[12] Vegard L 1921 *Z. Phys.* **5** 17
[13] Ekstein H 1945 *Phys. Rev.* **68** 120
[14] Dederichs P H 1973 *J. Phys. F: Met. Phys.* **3** 471
[15] Peisl H 1975 *J. Appl. Crystallogr.* **8** 471
[16] Trinkaus H 1972 *Phys. Status Solidi* b **51** 307
[17] Landau L D 1986 *Theory of Elasticity* (Oxford: Pergamon)
[18] *Landolt–Börnstein New Series* 1987 Group III, vols 17a, 17b, 22a, ed O Madelung and M Schulz (Berlin: Springer)